Annals of Biomedical Engineering, Vol. 47, No. 1, January 2019 *(© 2018)* pp. 97–112
https://doi.org/10.1007/s10439-018-02129-5

A Non-Invasive Material Characterization Framework for Bioprosthetic Heart Valves

MOSTAFA ABBASI,[1] MOHAMMED S. BARAKAT,[1] DANNY DVIR,[2] and ALI N. AZADANI[1]

[1]The DU Cardiovascular Biomechanics Laboratory, Department of Mechanical and Materials Engineering, University of Denver, Denver, CO, USA; and [2]Department of Medicine, Division of Cardiology, University of Washington, Seattle, WA, USA

(Received 17 April 2018; accepted 11 September 2018; published online 18 September 2018)

Associate Editor Arash Kheradvar oversaw the review of this article.

Abstract—Computational modeling and simulation has become more common in design and development of bioprosthetic heart valves. To have a reliable computational model, considering accurate mechanical properties of biological soft tissue is one of the most important steps. The goal of this study was to present a non-invasive material characterization framework to determine mechanical propertied of soft tissue employed in bioprosthetic heart valves. Using integrated experimental methods (i.e., digital image correlation measurements and hemodynamic testing in a pulse duplicator system) and numerical methods (i.e., finite element modeling and optimization), three-dimensional anisotropic mechanical properties of leaflets used in two commercially available transcatheter aortic valves (i.e., Edwards SAPIEN 3 and Medtronic CoreValve) were characterized and compared to that of a commonly used and well-examined surgical bioprosthesis (i.e., Carpentier-Edwards PERIMOUNT Magna aortic heart valve). The results of the simulations showed that the highest stress value during one cardiac cycle was at the peak of systole in the three bioprostheses. In addition, in the diastole, the peak of maximum in-plane principal stress was 0.98, 0.96, and 2.95 MPa for the PERIMOUNT Magna, CoreValve, and SAPIEN 3, respectively. Considering leaflet stress distributions, there might be a difference in the long-term durability of different TAV models.

Keywords—Inverse finite element simulation, Bioprosthetic heart valves, Three-dimensional anisotropic mechanical properties, Optimization, Fung constitutive model, Holzapfel–Gasser–Ogden constitutive model, Carpentier-Edwards PERIMOUNT Magna, Edwards SAPIEN 3, Medtronic CoreValve.

Address correspondence to Ali N. Azadani, The DU Cardiovascular Biomechanics Laboratory, Department of Mechanical and Materials Engineering, University of Denver, Denver, CO, USA. Electronic mail: Ali.Azadani@du.edu

INTRODUCTION

Pre-clinical assessment and verification of life sustaining implantable medical devices such as prosthetic heart valves are essential and required by regulatory agencies. As a result, *in vitro* bench-top and pre-clinical animal testing have been employed to verify safety and improve design features of prosthetic heart valves.[30] However, the pre-clinical studies are time-consuming and costly, and therefore, the tests may potentially inhibit exploration and use of novel materials and designs in prosthetic heart valves. In the past few years, computational modeling and simulation have been widely employed to expedite design and optimization of new medical devices.[20,43] Computational simulations can play a pivotal role in design and development of prosthetic heart valves by reducing the need to perform expensive pre-clinical tests. Furthermore, regulatory agencies such as the U.S. Food and Drug Administration (FDA) and EU Medical Device Regulatory System currently accept validated computational modeling and simulation as a scientific evidence in regulatory submissions.[18]

In the past decade, use of bioprosthetic heart valves for aortic valve replacement has increased significantly.[39] The trend was due to promising improvements in the long-term durability of surgical aortic valves (SAVs) and the advent of transcatheter aortic valves (TAVs).[14,29] Randomized clinical trials proved transcatheter aortic valve replacement (TAVR) improved survival over medical therapy for inoperable patients with severe symptomatic aortic stenosis.[33,38,41,45,46] Furthermore, transfemoral TAVR showed equivalent or superior outcomes when compared to surgical aortic valve replacement (SAVR) for the high-risk[5,35,40,56] and intermediate-risk[37,48]

patients. At present, large randomized clinical trials are underway for low-risk surgical patients with aortic stenosis. However, durability is the Achilles heel of bioprosthetic heart valves.[7,12,17,21,32]

Accurate and validated computational simulations can be effectively used to improve structural and hemodynamic performance of bioprosthetic heart valves. The commercially available bioprosthetic heart valves are made form materials such as metals (e.g., stainless steel, cobalt alloys, and titanium-nickel alloy (Nitinol), polymers (e.g., Dacron and Teflon), and fixed biological soft tissue (e.g., bovine and porcine pericardium). To have a reliable computational model, considering accurate mechanical properties for the bioprosthetic materials is a crucial step. In the past few decades, mechanical properties of bovine and porcine pericardium have been obtained primarily using experimental methods such as uniaxial and biaxial tensile tests.[1,51,58] However, the planar tests cannot capture the out-of-plane mechanical behavior of the soft tissue and other deformation modes at physiological strain rates are required to obtain the out of plane properties.[25] In addition, due to extensive intra-specimen and inter-specimen variations,[23] mechanical properties of examined materials in the pre-clinical tests may be significantly different from the actual materials used in the implanted bioprosthetic valves. Consequently, employing optimized material parameters to describe valve-specific mechanical behavior of the leaflets is essential in computational simulations.

In the present study, we aimed to develop a non-invasive material characterization framework using integrated experimental and numerical methods to determine mechanical propertied of soft tissue employed in bioprosthetic heart valves. Accordingly, we characterized three-dimensional anisotropic mechanical properties of leaflets used in two commercially available TAVs (i.e., Edwards SAPIEN 3 and Medtronic CoreValve), and compared the results to that of a commonly used and well-examined surgical bioprosthesis (i.e., Carpentier-Edwards PERIMOUNT Magna aortic heart valve). In addition, the present work presents a reliable approach to compare leaflet stress distribution among different bioprostheses under physiological loading condition.

MATERIALS AND METHODS

In the present study, two commercially available TAVs and one surgical bioprosthesis with comparable size were evaluated (Fig. 1). The first bioprosthetic valve was a 25-mm Carpentier-Edwards (CE) PERIMOUNT Magna aortic heart valve (Edwards Lifesciences, CA). The surgical bioprosthetic valve was made from bovine pericardium leaflets mounted on an Elgiloy frame with an internal diameter of 24 mm. The second bioprosthesis was a self-expanding 26-mm Medtronic CoreValve (Medtronic, Minneapolis, MN), consists of porcine pericardial leaflets mounted on a self-expanding Nitinol stent. The third bioprosthetic valve investigated in this study was a 26-mm Edwards SAPIEN 3 (Edwards Lifesciences, Irvine, CA). The TAV was constructed from bovine pericardial leaflets mounted on a balloon-expandable cobalt-chromium stent. The thickness of the leaflets was measured using Mitutoyo Digital caliper (Mitutoyo Corp, Kanogawa, Japan) and the average thickness was 0.56, 0.43, and 0.32 mm for CE PERIMOUNT Magna bioprosthesis, CoreValve, and SAPIEN 3, respectively.

Experimental Setup

Digital Image Correlation Measurements

Due to the limited temporal and spatial resolution of the currently available *in vivo* imaging modalities, *in vitro* tests play a central role in characterizing mechanical properties of soft tissue and validate computational simulations. In view of that, high-resolution optical techniques such as digital image correlation (DIC) can be utilized to quantify bioprosthetic valve leaflet displacement non-invasively under a well-defined loading condition.[22] In this study, a high-resolution GOM-ARAMIS stereovision DIC system (GOM-Optical Measuring Techniques, Braunschweig, Germany) was used to obtain displacement map of the bioprosthetic heart valves. The system consists of two high-speed cameras with a resolution of 5 megapixels (2448 × 2050 pixels) equipped with 50 mm focal length Titanar lenses. The top side of the leaflets were sprinkled with graphite to create a speckled pattern (Fig. 2). Subsequently, the valves were stored in normal saline solution at the room temperature prior to the DIC measurements. Details of the DIC imaging and measurements have been previously described.[4] Briefly, the bioprosthetic valves were mounted inside an optically clear acrylic chamber on a custom-made fixture fabricated by U-Print SE Plus 3D printer (Stratasys Ltd., MN, USA). The valves were submerged fully in the chamber and the leaflets were pressurized uniformly from 20 mmHg to 120 mmHg using a peristaltic pump. A change in the pump speed resulted a corresponding change in the pressure within the testing chamber. Pressure in the chamber was measured continuously by a pressure transducer (Deltran, Utah Medical Products Inc., UT, USA), monitored by StatysTM software (BDC Laboratories, Wheat Ridge, CO, USA), and recorded simultaneously by a data acquisition system (NI SCC-68, National

FIGURE 1. (Left) 25-mm Carpentier-Edwards PERIMOUNT Magna surgical bioprosthetic aortic valve. (Center) 26-mm Medtronic CoreValve. (Right) 26-mm Edwards SAPIEN 3 transcatheter heart valve.

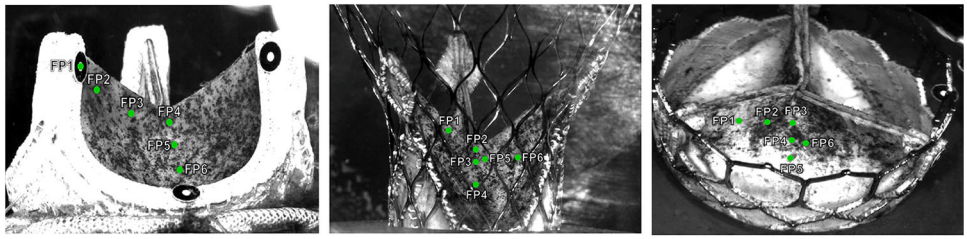

FIGURE 2. Example of speckled pattern and facets points that were used for post processing of the experimental data.

instruments, TX, USA). Pressure curves acquired from the DIC tests are shown in the supplementary materials (Supplementary Material 1). In addition, image acquisition was triggered simultaneously and image series were collected and stored using the ARAMIS DIC software (ARAMIS v2016, GOM, Braunschweig, Germany) at a frame rate of 10 frames per second. Following image acquisition, image processing was performed using the ARAMIS DIC software by discretizing all the images to a grid of square subsets of pixels called facet point (FP). An identical facet size (19 pixels) was considered for all the three valves. The number of facet points was approximately 180, 100, and 140 for CE PERIMOUNT Magna, CoreValve, and SAPIEN 3, respectively. A few sample FPs (FP1–FP6) are shown in Fig. 2. Leaflet deformation was determined by tracking the movement of the FPs. Three-dimensional surface contours of the displacement map were determined with respect to a reference pressure configuration, i.e., chamber pressure of 30-mmHg.

In Vitro Pulse Duplicator System

The three bioprosthetic heart valves were also examined under dynamic physiological loading condition in a custom-built pulse duplicator system (BDC Labs, Wheat Ridge, CO). Details of the *in vitro* tests have been previously described.[9,60] The pulse duplicator input parameters matched the international standard ISO 5840: 2015 recommendations for testing prosthetic heart valves, i.e., heart rate of 70 beats/min, mean atrial and aortic pressures of 10 and 100 mmHg, and cardiac output of 5 L/min. The physiological flow condition was simulated by controlling local compliance and peripheral resistance in the pulse duplicator. Recirculating fluid of 45% by volume glycerin solution (99% glycerin, The Science Company, Denver, CO) in phosphate buffered normal saline solution (PBS 100 ml tablets, Research Products International, Mount Prospect, IL) was used as a blood analog fluid at 37 °C. Pressure was measured in the aorta and left ventricle using strain gauge pressure transducers (Utah Medical Products, Midvale, UT, USA) embedded inside the pulse duplicator. The pressure transducers were calibrated prior to the tests using Delta-Cal Pressure transducer simulator/tester (Utah Medical Products, Inc.). SAPIEN 3 was implanted in a custom-built silicone washer and the valve was balloon-expanded to its nominal diameter. Details of the *in vitro* tests were previously described in Barakat *et al.*[9] Transvalvular pressure waveform and flow rate of the three bioprosthetic valves were measured from the *in vitro* tests (Supplementary Material 2). Furthermore, the leaflet motion for the valves was captured by a using a high-speed camera, SONY DSC-RX10M3 high-speed camera, at a rate of 960 frames per second. The images were digitized in MATLAB, and the center of each leaflet was tracked and its distance with respect

to the center of the three valves was calculated through the entire cardiac cycle.

Computational Simulation

Finite Element Modeling

Leaflet geometry of the three bioprosthetic valves was obtained using NextEngine 3D Laser Scanner with a resolution of 100 micrometers (NextEngine, Inc., Santa Monica, CA). In each scan, TAV stents block (optical) access to certain regions of the leaflets. Therefore, multiple scans from different angles were collected and fused together in the Next-Engine software. Surface reconstruction of valves was performed using RapidWorks and SOLIDWORKS packages. Reconstruction of the leaflets geometry was based one single leaflet and the other two leaflets were added using symmetry. IGES format of the leaflets were obtained for finite element (FE) simulations. For mesh generation, the leaflets were imported to HyperMesh (Altair Engineering, Inc., Troy, MI), and the geometry was discretized using a mapped mesh. The mesh was subsequently imported to ABAQUS/Explicit solver. The leaflet thickness was assumed uniform and constant throughout the leaflet. Material orientation was assigned to the shell elements using a home-developed MATLAB code. Density of the leaflets was considered to be 1100 kg/m^3.[34] Frame of the surgical bioprosthetic valve was found to be flexible in the DIC tests.[4] Therefore, a flexible frame with a uniform diameter, measured by the caliper to be 0.89 mm, and density of 8300 kg/m^3[50] was considered in the FE simulations for the surgical bioprosthesis (Fig. 3). Due to the high radial strength of TAV frames, the stent of CoreValve and SAPIEN 3 was considered to be rigid. The rigidity of the TAV frames was confirmed by the DIC measurements. The geometry of CE PERIMOUNT Magna bioprosthesis was meshed using 7674 ABAQUS S4 shell elements and 345 B31 beam elements. The beam elements of the surgical valve frame were connected to the leaflet using multi-point constraints. Besides, 11,166 and 8250 ABAQUS S4 shell elements were used to discretize CoreValve and SAPIEN 3 bioprostheses, respectively. The number of elements in the simulations was adequate to assure that the results are independent of mesh density, with a difference less than 1%. The mesh sensitivity analysis was based on comparison of the maximum displacement of the middle point of the leaflet's free-edge and its maximum principle stress value. Transvalvular pressure gradient waveforms obtained from the *in vitro* tests were applied to the ventricular side of the leaflets. Moreover, a Rayleigh damping coefficient α was introduced to the simulations to mimic viscous damping effects of surrounding fluid.

In the FE simulations, bioprosthetic leaflets were considered to be pseudo-hyperelastic anisotropic materials.[2,3] There are two forms of strain energy potentials available in ABAQUS/Explicit to characterize anisotropic materials: (i) generalized three-dimensional Fung strain-energy function proposed by Humphrey[27] and (ii) Holzapfel–Gasser–Ogden (HGO) strain energy function which was developed as a framework to model arterial layers with distributed collagen fiber orientation.[24] A generalized Fung strain-energy function is in the form

$$\Psi = \frac{c}{2}\left(e^{Q} - 1\right) + \frac{1}{\mathcal{D}}\left(\frac{J_{\mathrm{el}}^2 - 1}{2} - \ln J_{\mathrm{el}}\right) \tag{1}$$

where Ψ is the strain energy per unit of reference volume. $\mathcal{D}$ and c describe the temperature-dependent material parameters, J_{el} stands for the elastic volume ratio which is equal to J in the absence of thermal strains, and Q is given by

$$Q = E : (\mathbb{b}E) \tag{2}$$

where $\mathbb{b}$ is a non-dimensional symmetric fourth-order tensor with 21 independent components, and $\boldsymbol{E}$ is the Green–Lagrange strain tensor,.

$$\mathbb{b}_{\mathrm{anisotropic}} = \begin{bmatrix} b_{1111} & b_{1122} & b_{1133} & b_{1123} & b_{1113} & b_{1112} \\ & b_{2222} & b_{2233} & b_{2223} & b_{2213} & b_{2212} \\ & & b_{3333} & b_{3323} & b_{3313} & b_{3312} \\ & & & b_{2323} & b_{1323} & b_{1223} \\ & \text{Symmetric} & & & b_{1313} & b_{1213} \\ & & & & & b_{1212} \end{bmatrix} \tag{3}$$

Considering the incompressibility assumption ($J_{\mathrm{el}} = 1$), the Fung strain energy function is reduced to

$$\Psi = \frac{c}{2}\left(e^{Q} - 1\right) \tag{4}$$

On the other hand, the strain energy function for HGO model also known as Holzapfel model in ABAQUS consists of two terms: (i) isochoric and (ii) volumetric parts. The isochoric part is further decomposed into distinct matrix and fiber material terms with the following function

$$\Psi = \underbrace{\underbrace{C_{10}(\bar{I}_1 - 3)}_{matrix} + \underbrace{\frac{k_1}{2k_2}\sum_{\alpha=1}^{N}\{\exp[k_2\langle\bar{E}_\alpha\rangle^2] - 1\}}_{fiber}}_{isochoric} + \underbrace{\frac{1}{\mathcal{D}}\left(\frac{J_{\mathrm{el}}^2 - 1}{2} - \ln J_{\mathrm{el}}\right)}_{volumetric} \tag{5}$$

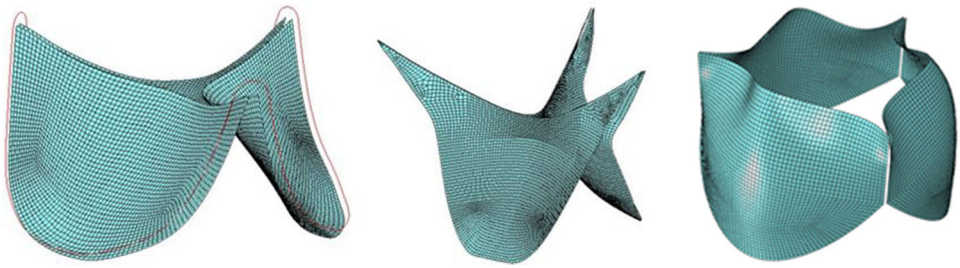

FIGURE 3. Representative FE models for (Left) Carpentier-Edwards PERIMOUNT Magna, (Center) Medtronic CoreValve, (Right) Edward SAPIEN 3.

With

$$\bar{E}_{\alpha} = \kappa(\bar{I}_1 - 3) + (1 - 3\kappa)\left(\bar{I}_{4(\alpha\alpha)} - 1\right) \qquad (6)$$

where C_{10} is the parameter of the isotropic neo-Hookean term which affects the stiffness of the isotropic hyperelastic matrix; k_1, k_2 are temperature-dependent material parameters which determine the stiffness and exponential response of the collagen fiber networks in the material, respectively; $\mathcal{D}$ is the compressibility parameter; κ describes the level of dispersion in the fiber directions ($0 \le \kappa \le 1/3$); N is the number of families of fibers ($N \le 3$); $\bar{I}_1$ is the first deviatoric strain invariant; and $\bar{I}_{4(\alpha\alpha)}$ are pseudo-invariants of the right Cauchy Green tensor and a set of unit vectors for the fiber directions. The structural anisotropy induced by the fiber network originates from $\bar{I}_{4(\alpha\alpha)}$. The HGO model can be defined by five parameters (C_{10}, k_1, k_2, κ, $\mathcal{D}$). In this study, $\mathcal{D}$ was assumed to be a constant value of 10^{-5} for the bioprosthetic valve leaflets.[42]

Optimization Framework

To determine 3D mechanical properties of the leaflets, a two-step global optimization approach was utilized. The flowchart in Fig. 4 shows how the optimization technique was implemented to find the material parameters. We used leaflet material properties reported in Abbasi *et al.*[3] and Martin and Sun[42] as initial estimate values of the optimization for Fung and HGO models, respectively. In the first step, the DIC measurements were utilized to determine leaflet material coefficients in both Fung and HGO models. The stent of CoreValve and SAPIEN 3 was considered to be rigid. However, for the surgical bioprosthesis a linear elastic frame was considered in the simulations. The Young's modulus of the frame was taken as an adjustable parameter in the optimization to match displacement of the frame obtained from the DIC tests. The Poisson's ratio of the frame was considered to be 0.226.[50] The material coefficients were obtained by minimizing the error norm of displacement field between DIC measurements and FE simulations for the six facet points, selected in the belly region and region close to the free edge of the leaflets as shown in Fig. 2, using particle swarm optimization (PSO)[8] method implemented in Isight (Simulia, Providence, RI). The number of facet points provided a right balance between the complexity of the analysis (i.e., computational cost) and accuracy of the computational model. Equal weight was considered for all the facet points. The objective function in the optimization procedure was average of the sum of the squared differences between the displacement values of the experimental results and simulation results. In the optimization procedure, DIC data obtained from a single leaflet per valve were used. The optimization process terminated when the change of the objective function was less than the set tolerance of 10^{-5}. Approximately, 500 iterations were performed to achieve convergence. The displacement contour plots obtained by the optimized material coefficients was then compared with experimental displacement contours obtained from the DIC tests. A material model that showed a good agreement with the experimental data was then considered for the second step of optimization. In the second step, the leaflet material parameters plus the viscous damping coefficient were optimized based on the raw (unfiltered) hemodynamic data (i.e., pressure waveforms) obtained from the pulse duplicator system using PSO method in Isight. The middle point distance of leaflets with respect to the center of the valve in the FE simulation was matched with the experimental measurements in the pulse duplicator system. A similar objective function was considered in the second step. To reduce computational cost, only one cardiac cycle was simulated and one leaflet motion was considered in the optimization procedure during valve opening and closing. The optimization process was set to be terminated when the change of the objective function was less than the set tolerance of 10^{-5}.

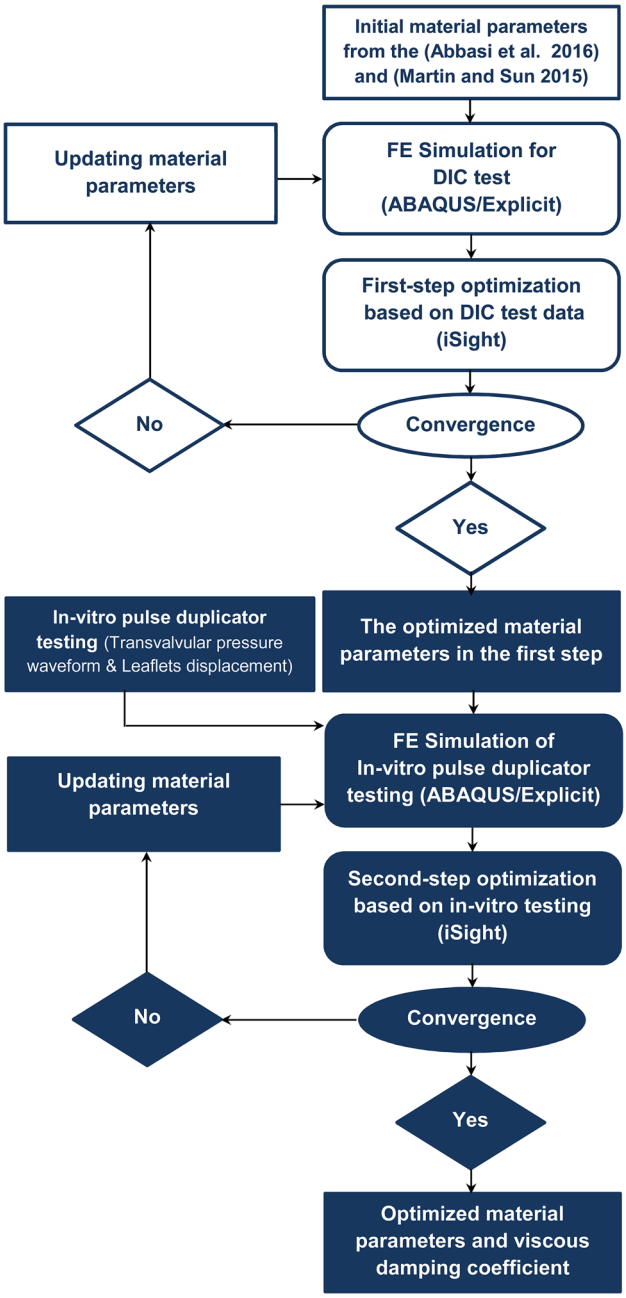

FIGURE 4. Flowchart for parameter estimation algorithm.

RESULTS

Estimated Material Parameters of Leaflets

The two-step optimization procedure was used to determine 3D mechanical properties of the bioprosthetic valve leaflets. First, DIC tests were simulated to obtain appropriate initial estimate values for the material coefficients in both Fung and HGO models. Material coefficients were obtained by minimizing the simulated and measured displacement vectors of the six facet points (Figs. 5a–5c). The results of material optimization are shown below for 3D anisotropic Fung model. Furthermore, the estimated values for c coefficient in the Fung model are presented in Table 1.

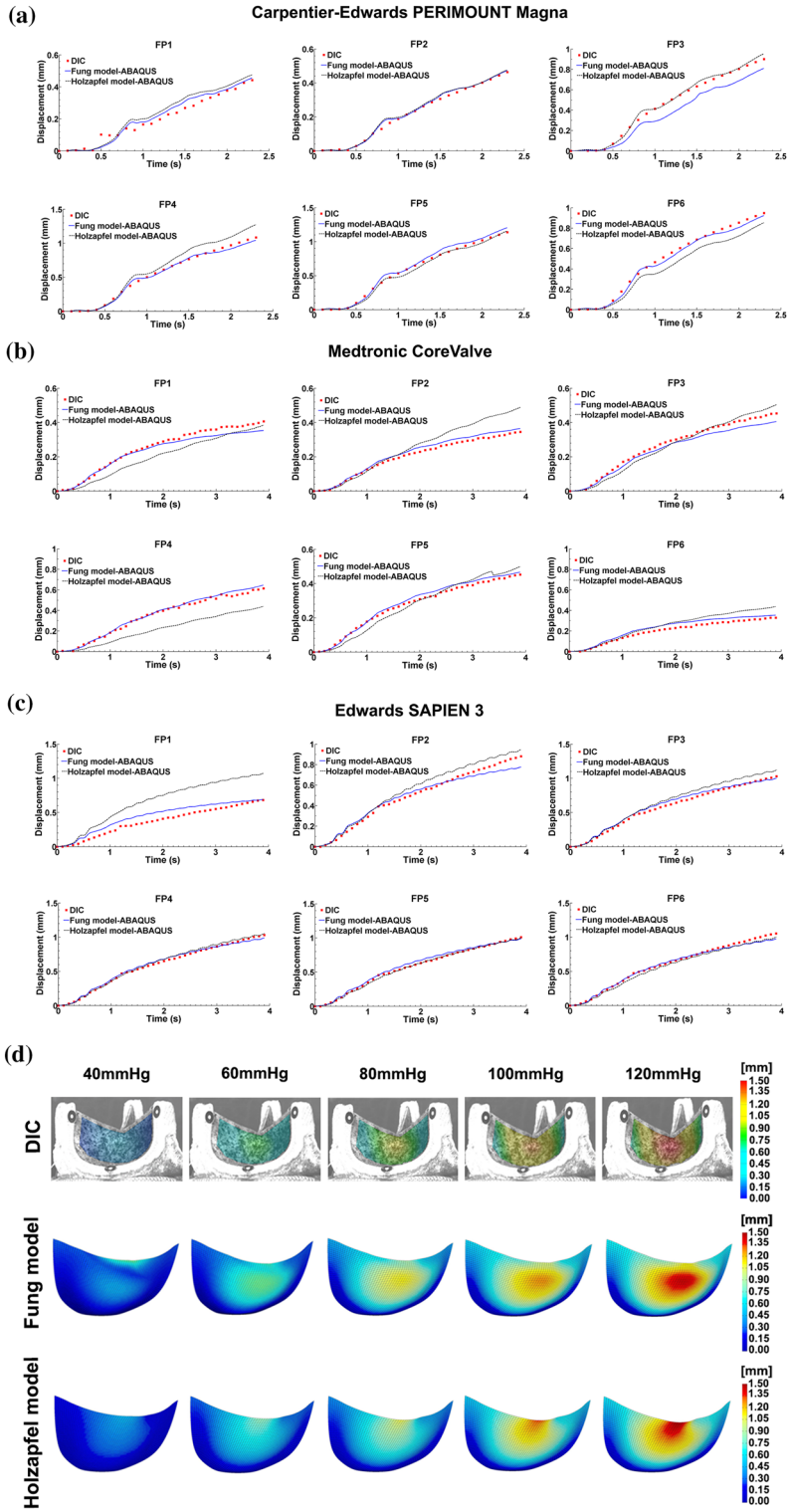

FIGURE 5. Displacement-time curves of the six facet points on the leaflets of (a) Carpentier-Edwards PERIMOUNT Magna, (b) Medtronic CoreValve, (c) Edward SAPIEN 3. (d) Comparison of displacement contour plots of PERIMOUNT Magna leaflets obtained from the FE simulations and DIC test at pressures of 40, 60, 80, 100 and 120 mmHg.

TABLE 1. Material parameter (c) coefficient for the Fung model after the first-step of the optimization procedure.

Bioprosthesis	c (kPa)
CE PERIMOUNT Magna	171.10
CoreValve	105.53
SAPIEN 3	52.32

TABLE 2. Optimized Holzapfel–Gasser–Ogden model parameters after the first-step of the optimization procedure.

Bioprosthesis	c_{10} (kPa)	k_1 (kPa)	k_2	κ
CE PERIMOUNT Magna	1457.56	584.76	820.64	0.299
CoreValve	764.27	1166.40	3986.86	0.292
SAPIEN 3	1772.98	1058.47	984.19	0.287

TABLE 3. Optimization objective functions based on the DIC measurements.

Bioprosthesis	Fung	Holzapfel–Gasser–Ogden
CE PERIMOUNT Magna	5.43E−06	1.43E−05
CoreValve	1.55E−06	4.41E−06
SAPIEN 3	3.77E−06	1.92E−05

$$\mathbb{b}_{\text{PERIMOUNT Magna (First-step optimization estimate)}} = \begin{bmatrix} 65.24 & 32.75 & 52.28 & 17.47 & 48.74 & 38.88 \\ & 62.51 & 46.69 & 67.17 & 65.73 & 20.02 \\ & & 61.28 & 38.03 & 62.67 & 53.36 \\ & & & 14.89 & 15.58 & 27.96 \\ & \text{Symmetric} & & & 45.49 & 14.26 \\ & & & & & 69.73 \end{bmatrix}$$

$$\mathbb{b}_{\text{CoreValve (First-step optimization estimate)}} = \begin{bmatrix} 64.10 & 38.52 & 57.15 & 18.84 & 45.21 & 47.59 \\ & 63.35 & 46.36 & 61.87 & 60.38 & 25.54 \\ & & 71.17 & 41.68 & 70.03 & 58.04 \\ & & & 15.90 & 14.90 & 28.00 \\ & \text{Symmetric} & & & 44.06 & 17.75 \\ & & & & & 66.33 \end{bmatrix}$$

.

$$\mathbb{b}_{\text{SAPIEN 3 (First-step optimization estimate)}} = \begin{bmatrix} 87.27 & 38.19 & 56.26 & 18.40 & 45.47 & 37.23 \\ & 83.97 & 43.50 & 70.21 & 71.65 & 25.72 \\ & & 92.84 & 43.70 & 62.41 & 58.98 \\ & & & 14.25 & 14.90 & 27.96 \\ & \text{Symmetric} & & & 44.84 & 17.70 \\ & & & & & 68.76 \end{bmatrix},$$

In addition, the results of material optimization for HGO model are shown in Table 2. For the three bioprosthetic heart valves, the curve fit of the generalized Fung model was to some extent better than the HGO model (Figs. 5a–5c and Table 3). In addition to the six facet points, to evaluate the overall accuracy of the two constitutive models, displacement contour plots of the leaflets were obtained from the FE simulations and compared with the displacement contour plots obtained from the DIC tests. As shown in Fig. 5d, the anisotropic Fung model simulated the surgical valve leaflet displacement better than the HGO model. Therefore, at the end of first step of the optimization, between the two constitutive models, the 3D anisotropic Fung model was chosen for the second step of the optimization procedure.

In the second step, bioprosthetic leaflet deformation was simulated under dynamic physiological loading condition that was obtained from *in vitro* tests in the pulse duplicator system. The range of initial values in the second step of the optimization was $0.8\times\ \mathbb{Z}_{(\text{First-step optimization estimate})} \le \mathbb{b} \le 1.2\times\ \mathbb{b}_{(\text{First-step optimization estimate})}$, $0.9 \times c_{(\text{First-step optimization estimate})} \le c \le 1.2\times\ c_{(\text{First-step optimization estimate})}$, and $1000 \le \alpha \le 11{,}000$. Three-dimensional generalized anisotropic Fung model parameters of the leaflets and Rayleigh damping coefficient for the three bioprostheses were estimated using PSO method in Isight by matching the middle point distance of one leaflet in the FE simulations with the averaged experimental data (Fig. 6). To reduce computational cost, only one leaflet motion was considered in the optimization procedure. After another 500 iterations, the optimization results showed a reasonable agreement with the experimental data. In addition, in Fig. 6, the results obtained from the optimized material parameters were compared to simulation results of using simply the initial material properties, described in the materials and methods section. A significant difference was observed both in term of its magnitude and timing. The difference between maximum opening value of the two simulations was 14.6, 14.2 and 24.8% for the CE PERIMOUNT Magna, CoreValve, and SAPIEN 3, respectively. The estimated material parameters of the leaflets for the three heart valves are listed below for the 3D anisotropic Fung model. In addition, the estimated values for c and the viscous damping coefficient are presented in Table 4.

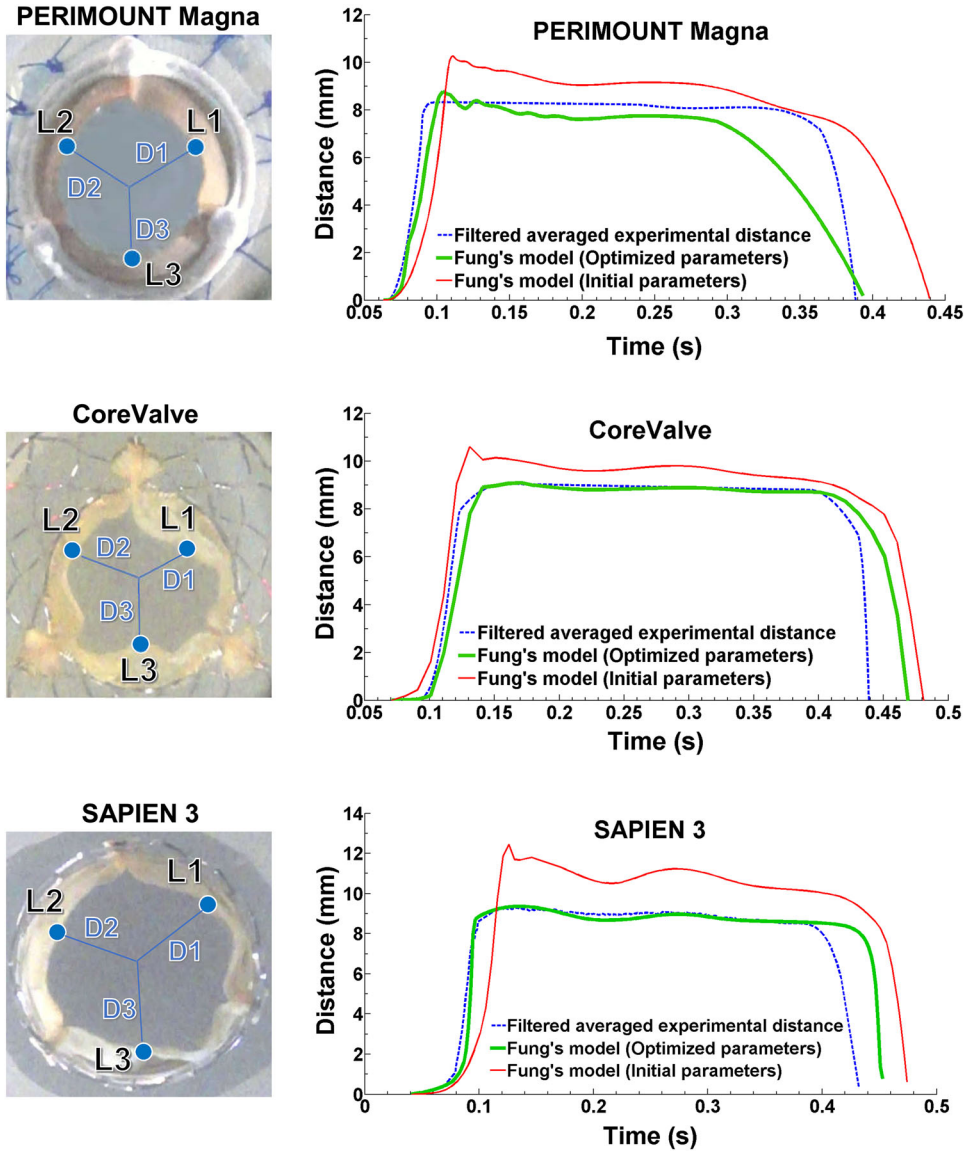

FIGURE 6. Middle point displacement of the leaflet for the three valves; comparing optimized FE simulations with the experimental data. The average standard deviation for the three leaflets based on the experimental data was ± 0.38, ± 0.35, and ± 0.18 mm for the CE PERIMOUNT Magna, CoreValve, and SAPIEN 3, respectively.

TABLE 4. Material parameter and viscous damping coefficient for 3D anisotropic Fung model.

Bioprosthesis	*c* (material parameter, *kPa*)	α (viscous damping, *1/s*)
CE PERIMOUNT Magna	90.72	10,642
CoreValve	100.29	8313
SAPIEN 3	47.53	4800

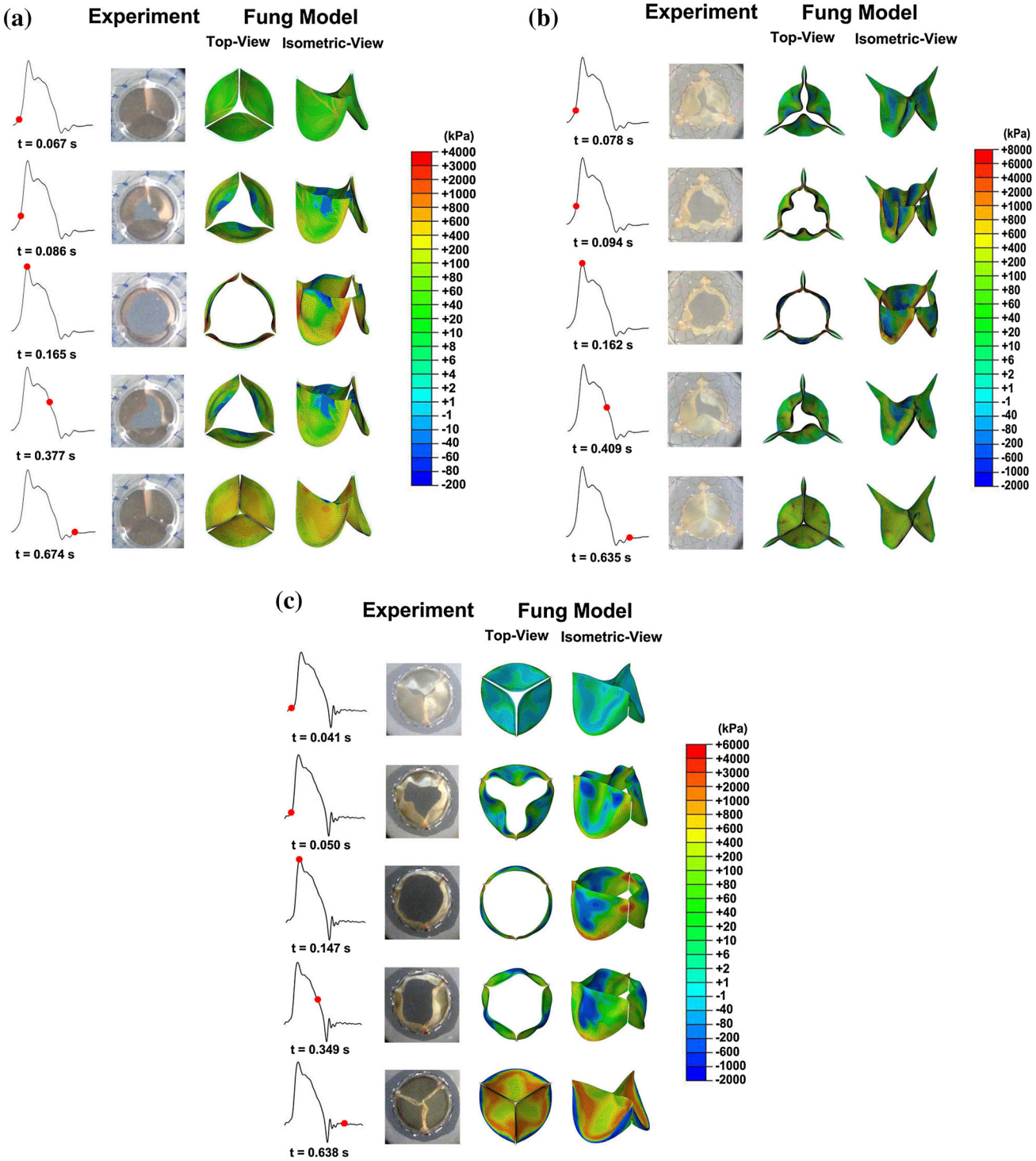

FIGURE 7. Comparison of *in vitro* leaflet motion with FE simulations throughout a complete cardiac cycle for the valves. The left plot represents flow curve. (Left column) Experimental data (Middle and right columns) the maximum principal stress distributions on the valve based on Fung-anisotropic model. (a) Carpentier-Edwards PERIMOUNT Magna, (b) Medtronic CoreValve, (c) Edward SAPIEN 3.

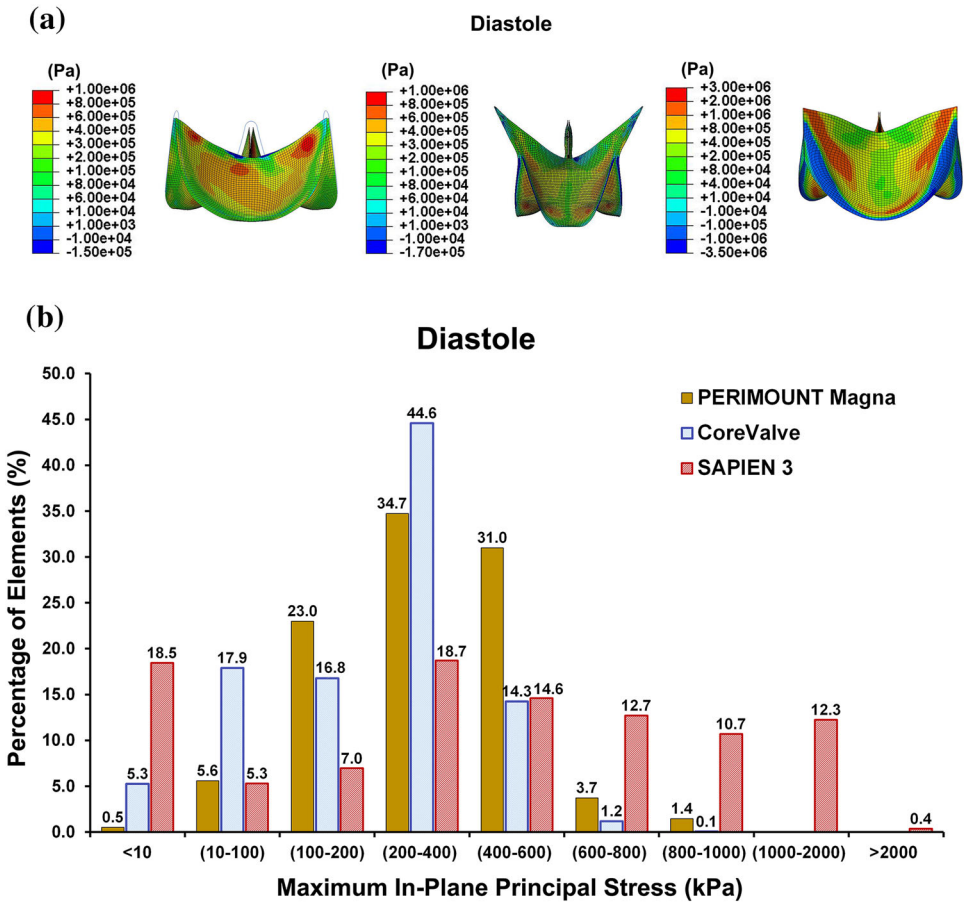

FIGURE 8. (a) Maximum in-plane principal stress contour plots of (Left) Carpentier-Edwards PERIMOUNT Magna, (Center) Medtronic CoreValve, (Right) Edward SAPIEN 3 at an identical pressure gradient of 16 kPa (≈ 120 mmHg). (b) The maximum in-plane principal stress histogram of the leaflets.

$$\mathbb{b}_{\text{PERIMOUNT Magna (estimated values)}} = \begin{bmatrix} 63.42 & 31.84 & 51.29 & 17.37 & 49.02 & 39.39 \\ & 63.74 & 46.75 & 68.38 & 63.09 & 19.22 \\ & & 62.82 & 38.51 & 60.17 & 55.50 \\ & & & 14.30 & 15.47 & 28.04 \\ & \text{Symmetric} & & & 47.30 & 13.69 \\ & & & & & 67.53 \end{bmatrix},$$

$$\mathbb{b}_{\text{CoreValve (estimated values)}} = \begin{bmatrix} 64.10 & 38.51 & 57.14 & 18.89 & 44.91 & 47.58 \\ & 63.25 & 45.96 & 62.37 & 61.13 & 25.19 \\ & & 71.65 & 42.18 & 69.83 & 58.04 \\ & & & 15.45 & 14.33 & 27.93 \\ & \text{Symmetric} & & & 43.87 & 17.01 \\ & & & & & 66.12 \end{bmatrix},$$

$$\mathbb{b}_{\text{SAPIEN 3 (estimated values)}} = \begin{bmatrix} 87.45 & 37.88 & 56.25 & 18.49 & 45.47 & 37.23 \\ & 83.97 & 43.50 & 70.21 & 71.65 & 25.72 \\ & & 89.93 & 43.70 & 62.41 & 58.98 \\ & & & 13.92 & 15.12 & 27.96 \\ & \text{Symmetric} & & & 43.54 & 16.47 \\ & & & & & 68.56 \end{bmatrix}.$$

Leaflet Stress Distribution

Using the optimized parameters, the maximum in-plane principal stress distribution of 25-mm CE PERIMOUNT Magna, 26-mm CoreValve, and 26-mm SAPIEN 3 were obtained and shown separately in Fig. 7a, 7b, and 7c, respectively. Two cardiac cycles were simulated to guarantee cycle invariance. The left-side columns depict the images of valve opening and

closing in the pulse duplicator, captured by the high-speed camera. In the systole, high stress regions were primarily observed in the fixed boundary edges of the three bioprostheses. The peak leaflet stress value during systole for the CE PERIMOUNT Magna, CoreValve, and SAPIEN 3 reached to 3.29, 7.25 and 7.53 MPa, respectively. During diastole, the peak stress value of the PERIMOUNT Magna, CoreValve, and SAPIEN 3 leaflets reached to 0.99, 1.01 and 2.53 MPa, respectively. In CE PERIMOUNT Magna and Edwards SAPIEN 3, the high stress regions were observed close to the commissures in the fully closed position. For Medtronic CoreValve, however, the maximum stress values were observed in the lower leaflet belly region.

To compare the leaflet stress distribution among the three bioprostheses, contours of maximum in-plane principal stress of the leaflets were determined at an identical pressure gradient in the diastole (i.e., 16 kPa). As shown in Fig. 8a, the peak of maximum in-plane principal stress was 0.98, 0.96 and 2.95 MPa for the CE PERIMOUNT Magna, CoreValve, and SAPIEN 3, respectively. Moreover, to quantify the difference in stress distribution among the three valves at the identical pressure gradient, the maximum in-plane principal stress histogram of the leaflets was presented in Fig. 8b. SAPIEN 3 had significantly more elements with stress values higher than 600 kPa (35.7%) compared to the PERIMOUNT Magna and CoreValve. In addition, 12.7% of elements in SAPIEN 3 had stress values higher than 1000 kPa (1 MPa). On the other hand, 94.9 and 98.7% of elements in the CE PERIMOUNT Magna and CoreValve had stress values of less than 600 kPa, respectively.

DISCUSSION

In the present study, we presented a non-invasive material characterization framework to determine mechanical propertied of soft tissue employed in bioprosthetic heart valves. We characterized three-dimensional anisotropic mechanical properties of leaflets used in two commercially available TAVs (i.e., Edwards SAPIEN 3 and Medtronic CoreValve), and compared the results to that of a commonly used and well-examined surgical bioprosthesis (i.e., Carpentier-Edwards PERIMOUNT Magna aortic heart valve). High resolution DIC was used to quantify bioprosthetic valve leaflet displacement under a well-defined loading condition. In addition, the bioprosthetic valves were examined under dynamic physiological loading condition in a pulse duplicator system. A two-step iterative optimization approach was then utilized to determine 3D anisotropic mechanical properties of the leaflets. Using the optimized material parameters, the maximum in-plane principal stress distribution of the three bioprostheses were obtained and compared during both systole and diastole.

In the past few years, use of bioprosthetic valves for aortic valve replacement has increased considerably.[39] To choose an appropriate bioprosthetic heart valve for aortic valve replacement, long-term durability of tissue heart valves is an important factor. Especially, to expand the reach of TAVR into low-risk younger patients, long-term durability of TAVs must be comparable to surgical bioprostheses. In surgical bioprosthetic valves, leaflets degenerate through two distinct but potentially synergistic mechanisms: (i) calcification and (ii) fatigue-induced structural deterioration (please see Supplementary Material 3).[53,54] Since the commercially available TAV leaflets are made from chemically treated bovine or porcine pericardium tissue, it can be postulated that the structural deterioration of TAVs occurs *via* the two failure mechanisms. Although, a unified definition of structural valve degeneration does not exist in the literature, the rate of structural valve degeneration in surgical bioprostheses is known to be less than 15% at 10 years.[49] In a retrospective cohort study, Forcillo *et al.*[19] studied 2405 patients with a mean age of 71 ± 9 years old who underwent aortic valve replacement with Carpentier-Edwards surgical pericardial bioprostheses. They found that the overall freedom rate of valve reoperation for valve dysfunction averaged 96 ± 1 and 67 ± 4% at 10 and 20 years, respectively. In addition, it is well known that the rate of reoperation for surgical valve dysfunction is strongly affected by age. Bourguignon *et al.*[13] showed that the freedom from reoperation rates attributable to structural valve deterioration in patients aged 60 or younger who received CE PERIMOUNT aortic valve were 88.3 ± 2.4 and 38.1 ± 5.6% at 10 and 20 years, respectively. On the other hand, clinical data regarding long-term durability of TAVs beyond 5 years is still limited. Dvir *et al.*[16] recently demonstrated the estimated structural valve degeneration rate of Cribier-Edwards, Edwards SAPIEN, and Edwards SAPIEN XT was approximately 50% at 8 years. In addition, Toggweiler *et al.*[59] reported that 9.7% of living patients in the study had moderate prosthetic valve failure after 5 years. On the other hand, the 5-year rate of prosthesis failure was 1.4% with the Medtronic CoreValve device.[10]

Computational modeling and simulation can provide qualitative and quantitative insights into the durability of bioprosthetic heart valves.[47,52,57,62,63] In the presence of limited clinical follow-up data for TAVs, several computational simulations have been performed to obtain stress and strain distributions of TAV leaflets.[1–3,26,31,42,61] The simulation results

showed higher mechanical stress in TAVs compare to surgical bioprosthetic valves. The increased mechanical stress on the leaflets may explain the relatively higher rate of accelerated tissue degeneration and diminished long-term valve durability. Considering the results presented in this study, there might also be a difference in the long-term durability of different TAV models and designs, as previously observed in clinical studies.[10,59] However, due to the limited number of valves examined in this study, it is prudent not to over-interpret the simulation results. Variation in leaflet thickness and material properties exists in each one of the TAV models that could potentially affect leaflet stress distribution. As a result, the simulation results must be validated by retrospective cohort studies to confirm the findings in presence of calcification and other patient related factors.

Accuracy of computational modeling and simulations depends on the accuracy of the prescribed material properties for the fixed bovine and porcine pericardium leaflets.[28] Regional structural and compositional heterogeneity has been observed in pericardium leaflets.[11,51,55] 3-D anisotropic constitutive models should therefore be considered for the fixed-biological tissue to fully describe the three-dimensional mechanical properties of the leaflets. Non-invasive material characterization methods, such as the one presented in this paper and other published studies,[3,6,36,44] can be used to determine the out-of-plane and shear coefficients of the bioprosthetic heart valve leaflets. Furthermore, extensive intra-specimen and inter-specimen variations exist in mechanical properties of soft tissue.[23] However, variability in the material properties of the three leaflets was not considered in the simulations of the three bioprostheses to reduce computational cost, which should be considered as a limitation of this study. In addition, it is imperative to evaluate bioprosthetic heart valves under dynamic loading condition to elucidate failure mechanism in bioprostheses (e.g., please see Supplementary Material 3A, leaflet tear close to the fixed boundary edge). Simplified loading conditions, e.g., quasi-static loading, may not represent the true loading condition that the valves are exposed to following replacement in clinical practice. Moreover, experimental validation of the computational simulations should be an indispensable part of evaluation.

CONCLUSIONS

In summary, we developed a two-step optimization procedure to determine 3D anisotropic mechanical properties of pericardial valves under physiological loading conditions. Three different bioprosthetic heart valves with comparable size were investigated. The optimized material parameters for each valve were implemented in FE simulations to assess the leaflet deformation and stress distribution. During systole, high stress regions were primarily observed at the boundary edge for the bioprostheses. However, during diastole, high stress regions were primarily observed in the commissures for CE PERIMOUNT Magna and Edwards SAPIEN 3. In contrary to the two other bioprostheses, the maximum stress values for the CoreValve were seen in the lower leaflet belly region. In addition, the CoreValve had the lowest peak stress value at the identical pressure value during diastole compared to the CE PERIMOUNT Magna and Edwards SAPIEN 3. The present work presents a reliable approach to compare leaflet stress distribution among different bioprostheses. Further studies are also motivated to obtain 3D anisotropic mechanical properties of pericardial leaflets under physiological loading condition using fluid–solid interaction simulations.

ELECTRONIC SUPPLEMENTARY MATERIAL

The online version of this article (https://doi.org/10.1007/s10439-018-02129-5) contains supplementary material, which is available to authorized users.

ACKNOWLEDGMENT

This work was supported partially by the American Heart Association Scientist Development Grant (AHA16SDG30920009) and by graduate scholarship from Jazan University.

REFERENCES

[1]Abbasi, M., and A. N. Azadani. Leaflet stress and strain distributions following incomplete transcatheter aortic valve expansion. *J. Biomech.* 48:3663–3671, 2015.

[2]Abbasi, M., and A. Azadani. Stress analysis of transcatheter aortic valve leaflets under dynamic loading: effect of reduced tissue thickness. *J. Heart Valve Dis.* 26:386–396, 2017.

[3]Abbasi, M., M. S. Barakat, K. Vahidkhah, and A. N. Azadani. Characterization of three-dimensional anisotropic heart valve tissue mechanical properties using inverse finite element analysis. *J. Mech. Behav. Biomed.* 62:33–34, 2016.

[4]Abbasi, M., Q. Qiu, Y. Behnam, D. Dvir, C. Clary, and A. N. Azadani. High resolution three-dimensional strain mapping of bioprosthetic heart valves using digital image correlation. *J. Biomech.* 76:27–34, 2018. https://doi.org/10.1016/j.jbiomech.2018.05.020.

[5]Adams, D. H., J. J. Popma, M. J. Reardon, S. J. Yakubov, J. S. Coselli, G. M. Deeb, T. G. Gleason, M. Buchbinder, J. Hermiller, Jr, N. S. Kleiman, S. Chetcuti, J. Heiser, W. Merhi, G. Zorn, P. Tadros, N. Robinson, G. Petrossian, G. C. Hughes, J. K. Harrison, J. Conte, B. Maini, M. Mumtaz, S. Chenoweth, J. K. Oh, and U. S. C. C. Investigators. Transcatheter aortic-valve replacement with a self-expanding prosthesis. *N. Engl. J. Med.* 370:1790–1798, 2014.

[6]Aggarwal, A., and M. S. Sacks. An inverse modeling approach for semilunar heart valve leaflet mechanics: exploitation of tissue structure. *Biomech. Model. Mechanobiol.* 15:909–932, 2016.

[7]Arsalan, M., and T. Walther. Durability of prostheses for transcatheter aortic valve implantation. *Nat Rev Cardiol* 13:360–367, 2016.

[8]Banks, A., J. Vincent, and C. Anyakoha. A review of particle swarm optimization. Part II: hybridisation, combinatorial, multicriteria and constrained optimization, and indicative applications. *Nat. Comput.* 7:109–124, 2008.

[9]Barakat, M., D. Dvir, and A. N. Azadani. Fluid dynamic characterization of transcatheter aortic valves using particle image velocimetry. *Artif. Organs* 2018. https://doi.org/10.1111/aor.13290.

[10]Barbanti, M., A. S. Petronio, F. Ettori, A. Latib, F. Bedogni, F. De Marco, A. Poli, C. Boschetti, M. De Carlo, and C. Fiorina. 5-year outcomes after transcatheter aortic valve implantation with CoreValve prosthesis. *JACC Cardiovasc. Interv.* 8:1084–1091, 2015.

[11]Billiar, K. L., and M. S. Sacks. Biaxial mechanical properties of the natural and glutaraldehyde treated aortic valve cusp—part I: experimental results. *J. Biomech. Eng.* 122:23–30, 2000.

[12]Bourguignon, T., A. L. Bouquiaux-Stablo, P. Candolfi, A. Mirza, C. Loardi, M. A. May, R. El-Khoury, M. Marchand, and M. Aupart. Very long-term outcomes of the Carpentier-Edwards Perimount valve in aortic position. *Ann. Thorac. Surg.* 99:831–837, 2015.

[13]Bourguignon, T., R. El Khoury, P. Candolfi, C. Loardi, A. Mirza, J. Boulanger-Lothion, A.-L. Bouquiaux-Stablo-Duncan, F. Espitalier, M. Marchand, and M. Aupart. Very long-term outcomes of the Carpentier-Edwards Perimount aortic valve in patients aged 60 or younger. *Ann. Thorac. Surg.* 100:853–859, 2015.

[14]Cribier, A., H. Eltchaninoff, A. Bash, N. Borenstein, C. Tron, F. Bauer, G. Derumeaux, F. Anselme, F. Laborde, and M. B. Leon. Percutaneous transcatheter implantation of an aortic valve prosthesis for calcific aortic stenosis first human case description. *Circulation* 106:3006–3008, 2002.

[15]Dvir, D., T. Bourguignon, C. M. Otto, R. T. Hahn, R. Rosenhek, J. G. Webb, H. Treede, M. E. Sarano, T. Feldman, and H. C. Wijeysundera. Standardized definition of structural valve degeneration for surgical and transcatheter bioprosthetic aortic valves. *Circulation* 137:388–399, 2018.

[16]Dvir, D., H. Eltchaninoff, J. Ye, A. Kan, E. Durand, A. Bizios, A. Cheung, M. Aziz, M. Simonato, and C. Tron. First look at long-term durability of transcatheter heart valves: assessment of valve function up to 10 years after implantation. *Eur. J. Cardiothorac Surg.*, 2016.

[17]Dvir, D., H. Eltchaninoff, J. Ye, A. Kan, E. Durand, A. Bizios, A. Cheung, M. Aziz, M. Simonato, C. Tron, Y. Arbel, R. Moss, J. Leipsic, H. Ofek, G. Perlman, M. Barbanti, M. Seidman, B. Philippe, R. Yao, R. Boone, S. Lauck, S. Lichtenstein, D. Wood, A. Cribier, and J. Webb. First look at long-term durability of transcatheter heart valves: assessment of valve function up to 10-years after implantation. In: EuroPCR 2016, Paris, France, 2016.

[18]Food and Drug Administration. Reporting of Computational Modeling Studies in Medical Device Submissions—Draft Guidance for Industry and Food and Drug Administration Staff only. Rockville, MD: Food and Drug Administration, 2014.

[19]Forcillo, J., M. Pellerin, L. P. Perrault, R. Cartier, D. Bouchard, P. Demers, and M. Carrier. Carpentier-Edwards pericardial valve in the aortic position: 25-years experience. *Ann. Thorac. Surg.* 96:486–493, 2013.

[20]Fries, R. C. Reliable Design of Medical Devices. Boca Raton: CRC Press, 2016.

[21]Grunkemeier, G. L., A. P. Furnary, Y. Wu, L. Wang, and A. Starr. Durability of pericardial versus porcine bioprosthetic heart valves. *J. Thorac. Cardiovasc. Surg.* 144:1381–1386, 2012.

[22]Heide-Jørgensen, S., S. K. Krishna, J. Taborsky, T. Bechsgaard, R. Zegdi, and P. Johansen. A novel method for optical high spatiotemporal strain analysis for transcatheter aortic valves in vitro. *J. Biomech. Eng.* 138:034504, 2016.

[23]Hiester, E. D., and M. S. Sacks. Optimal bovine pericardial tissue selection sites. I. Fiber architecture and tissue thickness measurements. *J. Biomed. Mater. Res.* 39:207–214, 1998.

[24]Holzapfel, G. A. Nonlinear Solid Mechanics: A Continuum Approach for Engineering. Chichester: Wiley, 2000.

[25]Holzapfel, G. A., and R. W. Ogden. On planar biaxial tests for anisotropic nonlinearly elastic solids. A continuum mechanical framework. *Math. Mech. Solids* 14:474–489, 2009.

[26]Hsu, M.-C., D. Kamensky, F. Xu, J. Kiendl, C. Wang, M. C. Wu, J. Mineroff, A. Reali, Y. Bazilevs, and M. S. Sacks. Dynamic and fluid–structure interaction simulations of bioprosthetic heart valves using parametric design with T-splines and Fung-type material models. *Comput. Mech.* 55:1211–1225, 2015.

[27]Humphrey, J. D. Mechanics of the arterial wall: review and directions. *Crit. Rev. Biomed. Eng.* 23:1–162, 1995.

[28]Humphrey, J. D. Continuum biomechanics of soft biological tissues. *Proc. R. Soc. A Math. Phys. Eng. Sci.* 459:3–46, 2003.

[29]Isaacs, A. J., J. Shuhaiber, A. Salemi, O. W. Isom, and A. Sedrakyan. National trends in utilization and in-hospital outcomes of mechanical versus bioprosthetic aortic valve replacements. *J. Thorac. Cardiovasc. Surg.* 149:1262e.3–1269e.3, 2015.

[30]ISO 5840-1:2015. Cardiovascular implants—cardiac valve prostheses—part 1: general requirements.

[31]Jermihov, P. N., L. Jia, M. S. Sacks, R. C. Gorman, J. H. Gorman, III, and K. B. Chandran. Effect of geometry on the leaflet stresses in simulated models of congenital bicuspid aortic valves. *Cardiovasc Eng Technol* 2:48–56, 2011.

[32]Johnston, D. R., E. G. Soltesz, N. Vakil, J. Rajeswaran, E. E. Roselli, J. F. Sabik, 3rd, N. G. Smedira, L. G. Svensson, B. W. Lytle, and E. H. Blackstone. Long-term durability of bioprosthetic aortic valves: implications from 12569 implants. *Ann. Thorac. Surg.* 99:1239–1247, 2015.

[33]Kapadia, S. R., M. B. Leon, R. R. Makkar, E. M. Tuzcu, L. G. Svensson, S. Kodali, J. G. Webb, M. J. Mack, P. S. Douglas, V. H. Thourani, V. C. Babaliaros, H. C. Herrmann, W. Y. Szeto, A. D. Pichard, M. R. Williams, G. P.

Fontana, D. C. Miller, W. N. Anderson, C. R. Smith, J. J. Akin, and M. J. Davidson. 5-year outcomes of transcatheter aortic valve replacement compared with standard treatment for patients with inoperable aortic stenosis (PARTNER 1): a randomised controlled trial. *Lancet* 385(9986):2485–2491, 2015.

[34]Kim, H., J. Lu, M. S. Sacks, and K. B. Chandran. Dynamic simulation pericardial bioprosthetic heart valve function. *J. Biomech. Eng.* 128:717–724, 2006.

[35]Kodali, S. K., M. R. Williams, C. R. Smith, L. G. Svensson, J. G. Webb, R. R. Makkar, G. P. Fontana, T. M. Dewey, V. H. Thourani, A. D. Pichard, M. Fischbein, W. Y. Szeto, S. Lim, K. L. Greason, P. S. Teirstein, S. C. Malaisrie, P. S. Douglas, R. T. Hahn, B. Whisenant, A. Zajarias, D. Wang, J. J. Akin, W. N. Anderson, and M. B. Leon. Two-year outcomes after transcatheter or surgical aortic-valve replacement. *N Engl J Med* 366:1686–1695, 2012.

[36]Lee, C.-H., R. Amini, R. C. Gorman, J. H. Gorman, and M. S. Sacks. An inverse modeling approach for stress estimation in mitral valve anterior leaflet valvuloplasty for in vivo valvular biomaterial assessment. *J. Biomech.* 47:2055–2063, 2014.

[37]Leon, M. B., C. R. Smith, M. J. Mack, R. R. Makkar, L. G. Svensson, S. K. Kodali, V. H. Thourani, E. M. Tuzcu, D. C. Miller, H. C. Herrmann, D. Doshi, D. J. Cohen, A. D. Pichard, S. Kapadia, T. Dewey, V. Babaliaros, W. Y. Szeto, M. R. Williams, D. Kereiakes, A. Zajarias, K. L. Greason, B. K. Whisenant, R. W. Hodson, J. W. Moses, A. Trento, D. L. Brown, W. F. Fearon, P. Pibarot, R. T. Hahn, W. A. Jaber, W. N. Anderson, M. C. Alu, and J. G. Webb. Transcatheter or surgical aortic-valve replacement in intermediate-risk patients. *N. Engl. J. Med.* 374:1609–1620, 2016.

[38]Leon, M. B., C. R. Smith, M. Mack, D. C. Miller, J. W. Moses, L. G. Svensson, E. M. Tuzcu, J. G. Webb, G. P. Fontana, R. R. Makkar, D. L. Brown, P. C. Block, R. A. Guyton, A. D. Pichard, J. E. Bavaria, H. C. Herrmann, P. S. Douglas, J. L. Petersen, J. J. Akin, W. N. Anderson, D. Wang, and S. Pocock. Transcatheter aortic-valve implantation for aortic stenosis in patients who cannot undergo surgery. *N. Engl. J. Med.* 363:1597–1607, 2010.

[39]Mack, M., and D. Holmes. Bioprosthetic valve thrombosis: the harder one looks, the more one finds. *J. Thorac. Cardiovasc. Surg.* 152:952–953, 2016.

[40]Mack, M. J., M. B. Leon, C. R. Smith, D. C. Miller, J. W. Moses, E. M. Tuzcu, J. G. Webb, P. S. Douglas, W. N. Anderson, E. H. Blackstone, S. K. Kodali, R. R. Makkar, G. P. Fontana, S. Kapadia, J. Bavaria, R. T. Hahn, V. H. Thourani, V. Babaliaros, A. Pichard, H. C. Herrmann, D. L. Brown, M. Williams, M. J. Davidson, L. G. Svensson, and J. Akin. 5-year outcomes of transcatheter aortic valve replacement or surgical aortic valve replacement for high surgical risk patients with aortic stenosis (PARTNER 1): a randomised controlled trial. *Lancet* 385(9986):2477–2484, 2015.

[41]Makkar, R. R., G. P. Fontana, H. Jilaihawi, S. Kapadia, A. D. Pichard, P. S. Douglas, V. H. Thourani, V. C. Babaliaros, J. G. Webb, H. C. Herrmann, J. E. Bavaria, S. Kodali, D. L. Brown, B. Bowers, T. M. Dewey, L. G. Svensson, M. Tuzcu, J. W. Moses, M. R. Williams, R. J. Siegel, J. J. Akin, W. N. Anderson, S. Pocock, C. R. Smith, and M. B. Leon. Transcatheter aortic-valve replacement for inoperable severe aortic stenosis. *N Engl J Med* 366:1696–1704, 2012.

[42]Martin, C., and W. Sun. Comparison of transcatheter aortic valve and surgical bioprosthetic valve durability: a fatigue simulation study. *J. Biomech. Eng.* 48:3026–3034, 2015.

[43]Morris, P. D., A. Narracott, H. von Tengg-Kobligk, D. A. S. Soto, S. Hsiao, A. Lungu, P. Evans, N. W. Bressloff, P. V. Lawford, and D. R. Hose. Computational fluid dynamics modelling in cardiovascular medicine. *Heart* 102:18–28, 2016.

[44]Murdock, K., C. Martin, and W. Sun. Characterization of mechanical properties of pericardium tissue using planar biaxial tension and flexural deformation. *J. Mech. Behav. Biomed. Mater.* 77:148–156, 2018.

[45]Nishimura, R. A., C. M. Otto, R. O. Bonow, B. A. Carabello, J. P. Erwin, 3rd, R. A. Guyton, P. T. O'Gara, C. E. Ruiz, N. J. Skubas, P. Sorajja, T. M. Sundt, 3rd, and J. D. Thomas. 2014 AHA/ACC Guideline for the Management of Patients With Valvular Heart Disease: a Report of the American College of Cardiology/American Heart Association Task Force on Practice Guidelines. *Circulation* 129:e521–643, 2014.

[46]Popma, J. J., D. H. Adams, M. J. Reardon, S. J. Yakubov, N. S. Kleiman, D. Heimansohn, J. Hermiller, Jr, G. C. Hughes, J. K. Harrison, J. Coselli, J. Diez, A. Kafi, T. Schreiber, T. G. Gleason, J. Conte, M. Buchbinder, G. M. Deeb, B. Carabello, P. W. Serruys, S. Chenoweth, J. K. Oh, and CoreValve United States Clinical Investigators. Transcatheter aortic valve replacement using a self-expanding bioprosthesis in patients with severe aortic stenosis at extreme risk for surgery. *J. Am. Coll. Cardiol.* 63:1972–1981, 2014.

[47]Rabkin, S. W., and P. H. Hsu. Mathematical and mechanical modeling of stress–strain relationship of pericardium. *Am. J. Physiol.* 229:896–900, 1975.

[48]Reardon, M. J., N. S. Kleiman, D. H. Adams, S. J. Yakubov, J. S. Coselli, G. M. Deeb, D. O'Hair, T. G. Gleason, J. S. Lee, J. B. Hermiller, Jr, S. Chetcuti, J. Heiser, W. Merhi, G. L. Zorn, 3rd, P. Tadros, N. Robinson, G. Petrossian, G. C. Hughes, J. K. Harrison, B. Maini, M. Mumtaz, J. V. Conte, J. R. Resar, V. Aharonian, T. Pfeffer, J. K. Oh, J. Huang, and J. J. Popma. Outcomes in the randomized CoreValve US pivotal high-risk trial in patients with a society of thoracic Surgeons risk score of 7% or less. *JAMA Cardiol* 1(8):945–949, 2016.

[49]Rodriguez-Gabella, T., P. Voisine, R. Puri, P. Pibarot, and J. Rodés-Cabau. Aortic bioprosthetic valve durability: incidence, mechanisms, predictors, and management of surgical and transcatheter valve degeneration. *J. Am. Coll. Cardiol.* 70:1013–1028, 2017.

[50]Roy, T., and A. Chanda. Computational modelling and analysis of latest commercially available coronary stents during deployment. *Procedia Mater. Sci.* 5:2310–2319, 2014.

[51]Sacks, M. S. Biaxial mechanical evaluation of planar biological materials. *J. Elasticity Phys. Sci. Solids* 61:199, 2000.

[52]Sacks, M. S., W. Zhang, and S. Wognum. A novel fibre-ensemble level constitutive model for exogenous cross-linked collagenous tissues. *Interface Focus* 6:20150090, 2016.

[53]Schoen, F. J. Mechanisms of function and disease of natural and replacement heart valves. *Annu. Rev. Pathol* 7:161–183, 2012.

[54]Schoen, F., R. Levy, A. Nelson, W. Bernhard, A. Nashef, and M. Hawley. Onset and progression of experimental

bioprosthetic heart valve calcification. *Lab. Invest.* 52:523–532, 1985.

[55]Simionescu, D., A. Simionescu, and R. Deac. Mapping of glutaraldehyde-treated bovine pericardium and tissue selection for bioprosthetic heart valves. *J. Biomed. Mater. Res. Part A* 27:697–704, 1993.

[56]Smith, C. R., M. B. Leon, M. J. Mack, D. C. Miller, J. W. Moses, L. G. Svensson, E. M. Tuzcu, J. G. Webb, G. P. Fontana, R. R. Makkar, M. Williams, T. Dewey, S. Kapadia, V. Babaliaros, V. H. Thourani, P. Corso, A. D. Pichard, J. E. Bavaria, H. C. Herrmann, J. J. Akin, W. N. Anderson, D. Wang, and S. J. Pocock. Transcatheter versus surgical aortic-valve replacement in high-risk patients. *N Engl J Med* 364:2187–2198, 2011.

[57]Soares, J. S., K. R. Feaver, W. Zhang, D. Kamensky, A. Aggarwal, and M. S. Sacks. Biomechanical behavior of bioprosthetic heart valve heterograft tissues: characterization, simulation, and performance. *Cardiovasc. Eng. Technol.* 7:309–351, 2016.

[58]Sun, W., A. Abad, and M. S. Sacks. Simulated bioprosthetic heart valve deformation under quasi-static loading. *J. Biomech. Eng.* 127:905–914, 2005.

[59]Toggweiler, S., K. H. Humphries, M. Lee, R. K. Binder, R. R. Moss, M. Freeman, J. Ye, A. Cheung, D. A. Wood, and J. G. Webb. 5-year outcome after transcatheter aortic valve implantation. *J. Am. Coll. Cardiol.* 61:413–419, 2013.

[60]Vahidkhah, K., M. Barakat, M. Abbasi, S. Javani, P. N. Azadani, A. Tandar, D. Dvir, and A. N. Azadani. Valve thrombosis following transcatheter aortic valve replacement: significance of blood stasis on the leaflets. *Eur. J. Cardiothorac. Surg.* 51:927–935, 2017.

[61]Xuan, Y., K. Krishnan, J. Ye, D. Dvir, J. M. Guccione, L. Ge, and E. E. Tseng. Stent and leaflet stresses in a 26-mm first-generation balloon-expandable transcatheter aortic valve. *J Thorac. Cardiovasc. Surg.* 153:1065–1073, 2017.

[62]Zhang, W., and M. S. Sacks. Modeling the response of exogenously crosslinked tissue to cyclic loading: the effects of permanent set. *J. Mech. Behav. Biomed. Mater.* 75:336–350, 2017.

[63]Zioupos, P., and J. Barbenel. Mechanics of native bovine pericardium: II. A structure based model for the anisotropic mechanical behaviour of the tissue. *Biomaterials* 15:374–382, 1994.